Optical Engineering 45(4), 046502 (April 2006)

Imaging quality analysis of a KBA x-ray microscope working at grazing incidence

Jiasheng Hu, MEMBER SPIE
Lingling Zhao
Xiang Li
Dalian University of Technology
School of Electronic and Information Engineering
Dalian 116024, China
E-mail: jshu@dlut.edu.cn

Yuhong Bai
Chinese Academy of Sciences
Changchun Institute of Optics, Fine Mechanics, and Physics
Changchun 130033, China

Abstract. In the last 20 years, x-ray imaging technology has developed to meet the needs of x-ray photoetching, spatial exploration, high-energy physics, and diagnosis of inertial confinement fusion. Because conventional imaging methods are not suitable in the x-ray range, grazing reflective imaging and coded aperture imaging methods have been adopted. In this paper, we describe the design of a noncoaxial grazing incidence KBA microscope. The microscope consists of two sets of spherical mirrors that scatter in orthogonal planes. An optical ray tracing program is used to analyze and evaluate the theoretical aberrations of the microscope. This allows us to optimize the x-ray imaging system. The analytical results provide a reliable foundation for determining the useful range and the manufacturing and assembly tolerances of the microscope.
[DOI: 10.1117/1.2188949]

Subject terms: x-ray imaging; KBA microscope; aberration analysis; grazing reflective imaging; quality evaluation.

Paper 040906RR received Nov. 30, 2004; revised manuscript received Jul. 28, 2005; accepted for publication Aug. 17, 2005; published online Apr. 27, 2006.

1 Introduction

Conventional visible-light imaging methods are not suitable for x-rays, for at least two reasons: (1) the index of refraction is very close to unity,[1] and (2) refractive imaging is almost impossible near normal incidence.

In 1922, Compton discovered that under grazing conditions x rays can reflect from polished surfaces, and total external reflection is observed.[2] In 1948, Kirkpatrick and Baez developed a grazing-reflection anastigmatic x-ray imaging system called a KB microscope (or telescope) that consists of two perpendicular spherical mirrors (or cylindrical surfaces) and utilizes the theory of total external reflection.[3] Although the KB microscope eliminates astigmatism, its field inclination and coma are very severe, restricting its development and applications.

In 1951, Wolter developed the Wolter I, Wolter II, and Wolter III telescope (or microscope) systems,[4] which extend the performance of grazing-reflection imaging systems. Unfortunately, it is difficult to make a Wolter-type microscope with good surface roughness because of its closed structure (surfaces of revolution are needed) and because it requires aspheric mirrors. The residual surface roughness also makes it difficult to apply the Wolter microscope for high-energy x-ray imaging because of the increase in scattering at shorter x-ray wavelengths.

The AKB system, developed by R. Kodama, Yosihio Suzuki, and others in 1989, is composed of two sets of KB systems to decrease the field inclination and correct aberrations. When aspheric mirrors are adopted in that system, although the imaging quality is improved, fabrication is quite difficult. Sauneuf et al. developed a new type of imaging system, called the KBA microscope (or telescope) (from French *KB amélioré*, meaning "improved KB") in 1997. The microscope consists of two sets of perpendicular spherical mirrors, each consisting of two parallel mirrors.[5,6] This system has advantages over other types of microscopes working at grazing incidence, such as increased field of view and easy fabrication.

In the last few decades, x-ray multilayer technology has developed fast, which makes normal-incidence x-ray imaging possible.[7–9] Recently, normal-incidence reflective x-ray microscopes using multilayer films at long wavelengths (soft x-ray range) have been demonstrated,[10] but challenges remain for applications in the medium and short wavelength ranges.

We have designed a KBA x-ray microscope, working at grazing incidence, to meet the requirements of the National Key Laboratory of Laser Fusion at the Chinese Academy of Engineering Physics, Mianyang, Sichuan. The purpose of the equipment is to characterize an inertial confinement fusion target exploded by a high-power laser. The equipment has been manufactured and assembled. The emphasis of the paper is on the computation and evaluation of the system aberrations described in a previous paper,[11] including spherical aberration, coma, astigmatism, and field obliquity. The analytical results provide a reliable basis for determining the useful spectral range, the manufacturing tolerances, and the assembly tolerances of the KBA microscope.

2 Imaging Characteristics of KBA X-Ray Microscope

KBA type microscopes as developed by Sauneuf et al. are composed of two pairs of spherical (or cylindrical) mirrors arranged so the pairs are perpendicular to each other. Each pair of spherical mirrors has two dispersive mirrors, as shown in Fig. 1. Because of the small glancing angle between the two mirrors they appear parallel. By making use

0091-3286/2006/$22.00

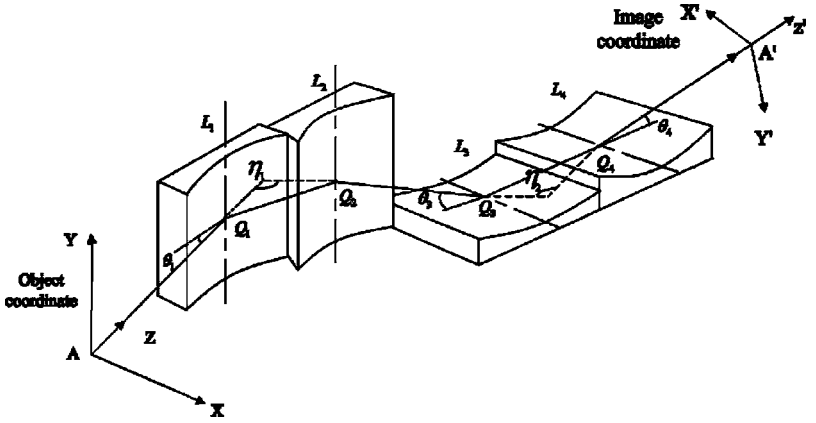

Fig. 1 KBA x-ray microscope.

of bimirror imaging characteristics, this kind of structure can reduce field obliquity, spherical aberration, and coma. Thus it can increase the effective field of view and improve the imaging quality.

In Fig. 1, the front pair of mirrors is composed of mirrors L_1 and L_2, with angle η_1. The back pair, perpendicular to the former, is composed of L_3 and L_4, with angle η_2. Here A is an object point, and A' is the corresponding image of A. The broken line $AQ_1Q_2Q_3Q_4A'$ is called the *pseudoaxis* of the system, and Q_1, Q_2, Q_3, Q_4 are the apices of the respective mirrors. The plane AQ_1Q_2 is horizontal, and that of Q_3Q_4A' is vertical. Off-axis thin rays near the pseudoaxis can be calculated from Young's equation:[1]

$$\frac{n'\cos^2 I'_p}{t'} - \frac{n\cos^2 I_P}{t} = \frac{n'\cos I'_P - n\cos I_P}{r}, \tag{1}$$

$$\frac{n'}{s'} - \frac{n}{s} = \frac{n'\cos I'_P - n\cos I_P}{r}. \tag{2}$$

Here t, s, t', and s' are the object distances and image distances formed by the meridian and sagittal rays, I_p, I'_p are incident angle and refractive (reflective) angle of the principle ray, n is the index of the front medium, n' is that of the back, and r is the curvature radius. If the imaging component is a mirror, $n'=-n=-1$, $I'_P=-I_P$, then (1) and (2) become

$$\frac{1}{t'} + \frac{1}{t} = \frac{1}{f'_t} = \frac{2}{r\sin\theta}, \tag{3}$$

$$\frac{1}{s'} + \frac{1}{s} = \frac{1}{f'_s} = \frac{2\sin\theta}{r}, \tag{4}$$

where θ is the grazing angle, with $\theta=90$ deg$-I_p$, and f'_t, f'_s are the focal lengths in the meridian plane and the sagittal plane, respectively.

The reflectivity increases as the glancing angle decreases. However, field obliquity and other aberrations become more severe as the glancing angle is decreased. We have designed the KBA system taking into account the working distance due to the implosion chamber size, the magnification determined from the pixel size of the x-ray detectors, and the state of the art of manufacturing mirrors[7] to reduce astigmatism and image inclination. This KBA x-ray microscope is designed to study inertial confinement fusion (ICF) in the Shenguang II laser facility at the National Key Laboratory of Laser Fusion. The system parameters are as follows:[11]

object distance $L=-220$ mm,

$\theta_1=\theta_2=1.6$ deg, $\theta_3=\theta_4=1.9$ deg,

$R=29$ m,

$Q_1Q_2=27$ mm, $Q_2Q_3=25$ mm, $Q_3Q_4=29$ mm,

and the solid angle in object space, $\omega=4\times10^{-6}$ sr.

The aperture stops in the meridian plane and the sagittal plane are placed separately in order to reduce the sizes of the mirrors and make the structure compact. Based on our modeling, we placed the stop on the second mirror in the meridian plane, and the stop on the fourth mirror in the sagittal plane.

The rays are traced on the basis of the preceding parameters using our own programs, and the final image distance is $L'_4=1786.73$. The magnification is $7.925\times$ in the horizontal plane (the meridian plane), and $6.2316\times$ in the vertical plane (the sagittal plane). The different magnifications in the two directions are caused by the difference between the focal lengths in the meridian plane and in the sagittal plane. This kind of error can be corrected by optical or digital processing.

3 Analysis of Aberrations

For the aberration analysis, we consider the rays in the horizontal and vertical planes separately. The incident rays in the horizontal plane (called simply meridional rays) are meridional rays for the front pair of mirrors, and become sagittal rays for the back one. The vertical incident rays (called simply sagittal rays) are sagittal for the front pair and become meridional for the back pair. Since the focal length in the sagittal plane is much longer than in the me-

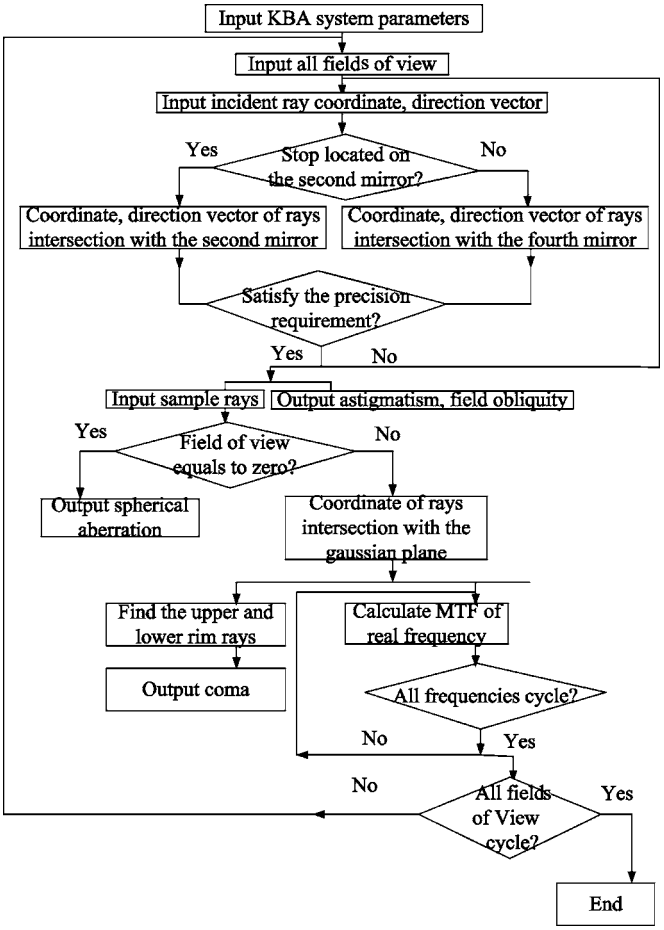

Fig. 2 Flow chart of the program.

ridian plane, the effect of the sagittal mirrors on the power can be ignored, and that is the reason that cylindrical mirrors can be substituted for spherical mirrors.[1] When the horizontal aberrations are calculated, we only consider the front pair of mirrors; when the vertical aberrations are calculated, only the back pair. The precision of this method for calculating aberrations is sufficient for evaluating imaging quality.

The design method for this kind of microscope system is discussed in our previous paper.[11] In this paper we are considering a double-separated-stop system, for which a general optical program is hardly suitable. We have compiled a special optical computing program for the system. We use this program to trace rays and calculate aberrations. When calculating rays and aberrations, the pseudoaxis is regarded as the optical axis, the stop in the meridian plane is on the second mirror, and the one in the sagittal plane is on the fourth mirror. The flow chart of the program is shown in Fig. 2.

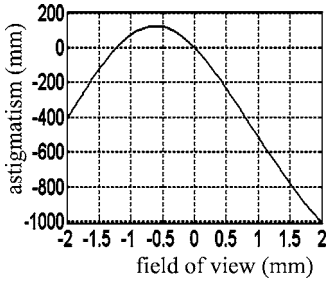

Fig. 3 KBA astigmatism.

3.1 *Astigmatism*

Astigmatism is the difference between focal point (or line) of meridian and sagittal paraxial rays of an off-axis object in image space and is the dominating aberration in an x-ray imaging system with a small solid angle. In the presence of astigmatism, a point source is imaged to two points (or lines) at separate distances. As shown in Sec. 2, the object distance of point A is 220 mm in the system. With the program we have optimized the design so the image distances in the meridional plane and the sagittal plane are 1786.71 and 1786.73 mm, respectively. This means that astigmatism is corrected in the system. We can see from Fig. 3 that the astigmatism is quadratic in the field of view and has an asymmetrical distribution relative to the optical pseudoaxis.

3.2 *Analysis of Field Obliquity*

The image formation of a single mirror is illustrated in Fig. 4, in which A and B are two object points, with A on the pseudoaxis, and A' and B' are their respective images. If $AB=0.5$ mm and the grazing incidence angle of point A is 1.6 deg, then the grazing incidence angle of point B is $1.6+180\times0.5/220\pi=1.7302$ deg. From (3) and (4), the focal lengths are $f'_A=404.863$ and $f'_B=437.804$, respectively. The image distance can be obtained by using Gauss's formula $1/l'-1/l=1/f'$. The results are $OA'=481.8144$ and $OB'=442.2200$. Thus the field obliquity is $\beta=88.41576$ deg. This means the image plane is severely inclined for a single mirror.

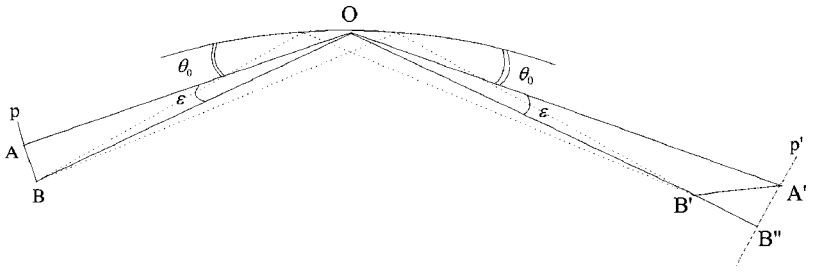

Fig. 4 Field obliquity of single mirror.

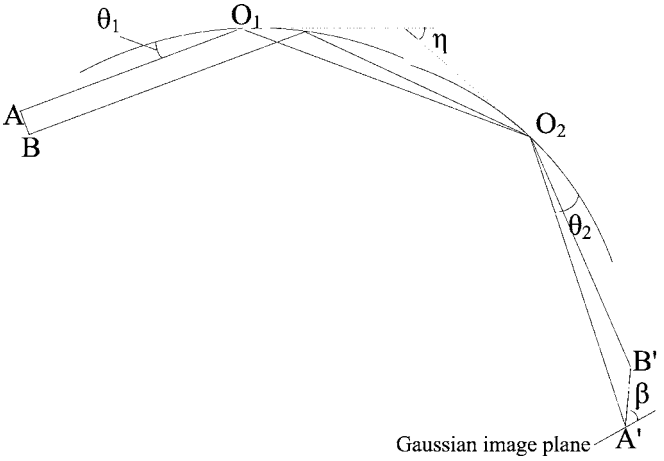

Fig. 5 Field obliquity of two mirrors.

The characteristic of double mirrors is used to reduce the field obliquity, as shown in Fig. 5. With two mirrors, the angle between incident rays and emergent rays is not changed, that is, it equals double the angle between the two mirrors, independent of the incident ray angle. Therefore we substitute two mirrors for the single spherical mirror.

In Fig. 4, we illustrate how a line perpendicular to AO is imaged to a line perpendicular to $A'O$. As shown, B is focused at B', but is a blurred disk at B''. The blur radius is $B''=2\times 39.6082u'=0.045$ mm (here $u'=0.000564$ is the aperture angle in image space). Obviously this blurring is unacceptable. If the angle between two plane mirrors is η ($\eta=\theta_1+\theta_2$), then the angle between the incident light beam and the emergent light beam is 2η whatever the incident angle is, as shown in Fig. 5. The angle between incident rays and emergent rays does not change. Thus the image plane $A'B'$ is approximately perpendicular to the optical axis, and the field obliquity is depressed. This is the main reason why the KBA system adopts two double mirrors. The field obliquity as a function of field of view is plotted in Fig. 6. The difference of field obliquity between the meridian line and sagittal line is caused by the asymmetry of the microscope system.

3.3 *Spherical Aberration*

Strictly speaking, incident rays are all off axis, and the pseudoaxis is regarded as the optical axis. The rays from point A are successively reflected by four mirrors in the KBA system, and finally, the different aperture rays intersect with the pseudoaxis at different locations. This deviation of image point distances between aperture rays and paraxial rays is called spherical aberration and expressed as $\delta L'=L'-l'$, as shown in Fig. 7. The transverse spherical aberration is written as $\delta T'=\delta L'\tan U'$. This value is the blur radius of longitudinal spherical aberration in the paraxial image plane. We can see from Fig. 8 that the transverse spherical aberration is asymmetrical, and the blur radius increases rapidly with aperture angle. In contrast with general optical systems, the longitudinal spherical aberration of this system is nearly linear in aperture angle; thus the transverse spherical aberration is nearly quadratic in aperture angle, and the linear approach error is smaller than 6%. Because aperture angles are smaller on the left than on the right in image space, transverse spherical aberrations are likewise smaller on the left.

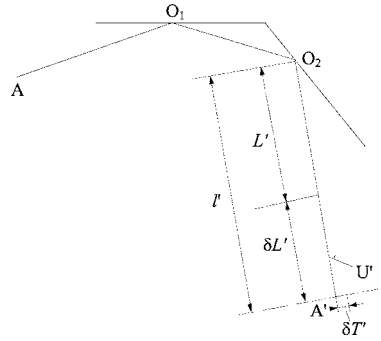

Fig. 7 Analysis of spherical aberration.

3.4 *Coma*

Coma is an aberration of an off-axis object that is a function of the aperture and the field of view in the optical system. The coma has an important effect on the imaging quality of an optical system, and there is no parameter for correcting aberrations in the KBA system. However, the coma is much lower for a KBA system than for a KB. In general the field of view of the KBA microscope is below 2 mm. The coma of the microscope is sensitive to the grazing incident angle, i.e., to the height of object. Here we

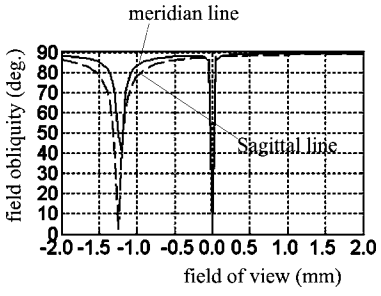

Fig. 6 KBA field obliquity.

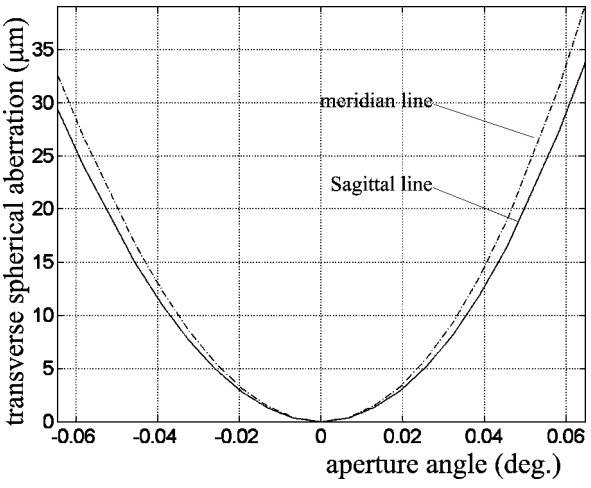

Fig. 8 Transverse spherical aberration.

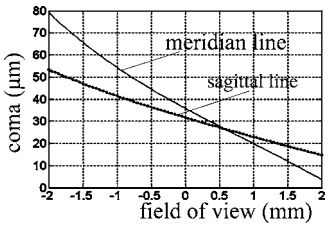

Fig. 9 System coma.

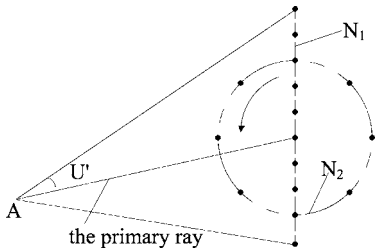

Fig. 10 Light-cone division.

mainly trace the principal ray and the upper and lower rim rays to determine the coma value for given field. The coma can be expressed as

$$K'_T = \frac{H'_1 + H'_2}{2} - H'_P,$$

where K'_T is the coma of the given field in the meridian plane, H'_1 and H'_2 are the image heights of the upper and lower rim rays, respectively, and H'_p is the image height of the principal ray. We can see from Fig. 9 that the coma is linear in the field height. This indicates that the third-order coma is dominant in the system. In a coaxial system, the tangential coma is generally 3 times as large as the sagittal coma. For the KBA microscope, however, there is not much difference between them, since the two sets of mirrors are perpendicular to each other and nonsymmetrical. As the field of view changes from −2 to +2 mm, the coma will decrease gradually, and the meridian coma and the sagittal coma will be nearly equal. The maximum values of the coma in the horizontal plane and the vertical plane are 79 and 53 μm, respectively.

4 Image Evaluation

4.1 *Spot Diagram and Encircled Energy*

As described in the preceding section, there are insufficient free parameters to correct all aberrations in the x-ray microscope. In order to minimize the aberrations, we determine the spot diagram and the modulation transfer function (MTF) for quantitatively evaluating the image quality of the system. This is valid for evaluation of systems with large aberration.

When the aberrations exceed the Rayleigh limit by several times, diffraction effects become insignificant, and the results of geometric ray tracing may be used to evaluate the appearance of a point image. This can be done by dividing the entrance pupil of the optical system into a large number of equal areas and tracing a ray from the object point through the center of each small area. The intersection of each ray with the selected image plane is plotted. Since each ray represents the same fraction of the total energy in the image, the density of the points in the plot is a measure of the power density (irradiance or illuminance) in the image. Obviously, the more rays are traced, the more accurate the expression of the geometrical image becomes. The ray intercept plot of this type is called a *spot diagram.*

Since it is difficult to accurately determine the entrance pupil position in the system, we divide the light-cone angle of an object point instead of using the method of entrance-pupil division. We first divide the cone angle (U=0.0646513 deg) into N_1 segments, then rotate these lines around the primary ray (pseudoaxis). We next divide every circle into N_2 segments. Therefore we need to trace altogether $N_1 \times N_2$ rays. This division method is illustrated in Fig. 10.

A few spot diagrams of different fields within ±2 nm are shown in Fig. 11, in which the horizontal coordinate represents the size of the spot diagram in the X' direction, and the vertical one represents the size in the Y' direction. The diagrams are plotted on the image plane perpendicular to the pseudoaxis with intercept A'. Figure 11(a) shows that the vertical blurring is almost independent of the horizontal blurring direction, and Fig. 11(b) vice versa. It is apparent that the severe asymmetrical distribution of the diagrams is a consequence of the fact that the system is noncoaxial. The coma of the system is very severe, and it restricts the effective field of view of the microscope. Figure 12(a) and 12(b) show the encircled energy plots corresponding to the

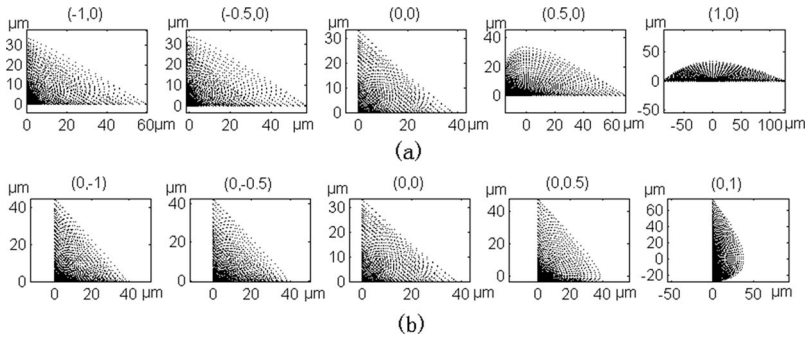

Fig. 11 Spot diagrams of different points (a) on *X* axis in meridional plane; (b) on *Y* axis in sagittal plane.

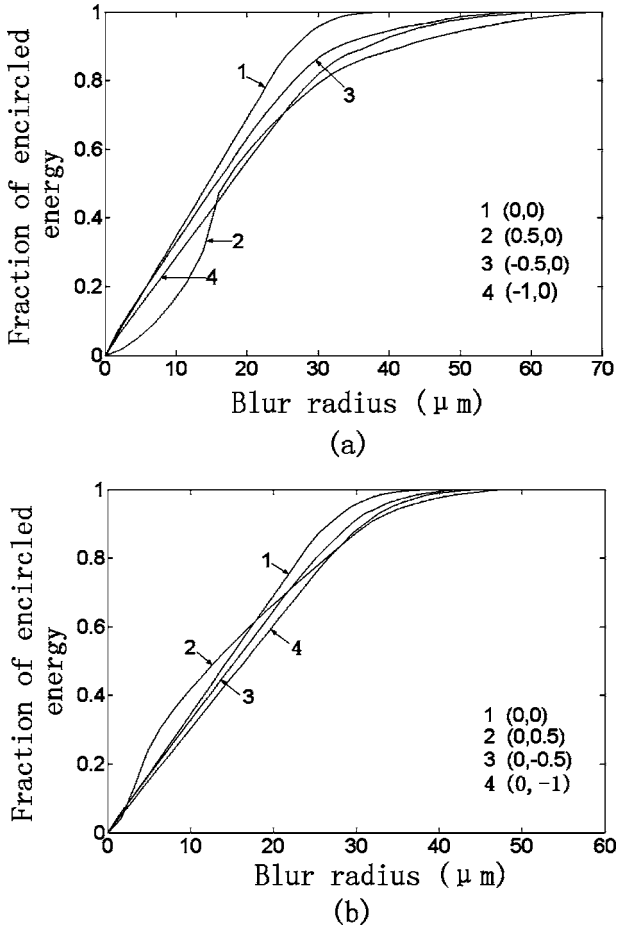

Fig. 12 Encircled energy of different field points in image space: (a) on *X* axis (b) on *Y* axis.

spot diagrams of Fig. 11. Since the x-ray microscope has large aberrations, the resolution criteria for small-aberration systems are not suitable for it. It is generally regarded that the circle enclosing 80% of the energy is the effective blurring spot, and the reciprocal of the blurring spot's diameter in millimeters is the resolvable spatial frequency of the system in line pairs per millimeter. From Fig. 12 we can see that about 80% of the power is concentrated within a 30-μm-diameter circle in the ±1-mm field of view. This shows that a resolution of 5 μm (200 lp/mm) for the object can be obtained.

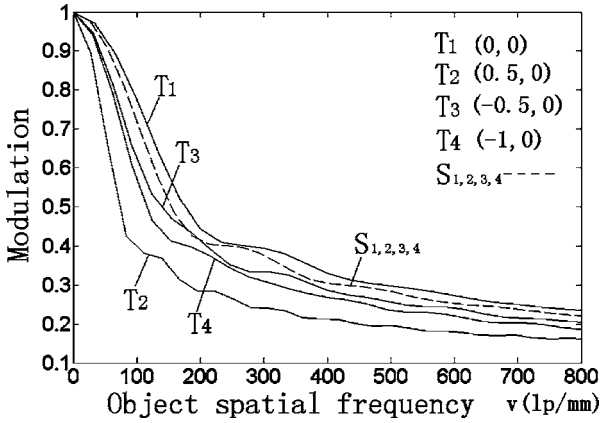

Fig. 14 The MTF curves with different field along the *X* axis.

4.2 *Optical Transfer Function*

The optical transfer function (OTF) indicates how different spatial frequencies are treated by an optical system, or by some other system, such as a film, CCD, or fiber. In other words, it represents the ability of an optical system to transfer information. Since the OTF can objectively and quantitatively indicate the imaging quality of an optical system, it is a frequently applied to imaging quality evaluation.[1] The OTF consists of the MTF and the phase transfer function (PTF). The MTF equals the modulation ratio between an object and its image at the same spatial frequency.

As shown in Sec. 4.1, the microscope is a large-aberration system, and its point spread function (PSF) is much larger than the diffraction-limited Airy disk. Therefore its PSF can be calculated by using spot diagrams.[12]

First of all, the spot diagram is divided into many small grid elements with equal intervals along the X' (or Y') direction. The number of spots within each grid element rep-

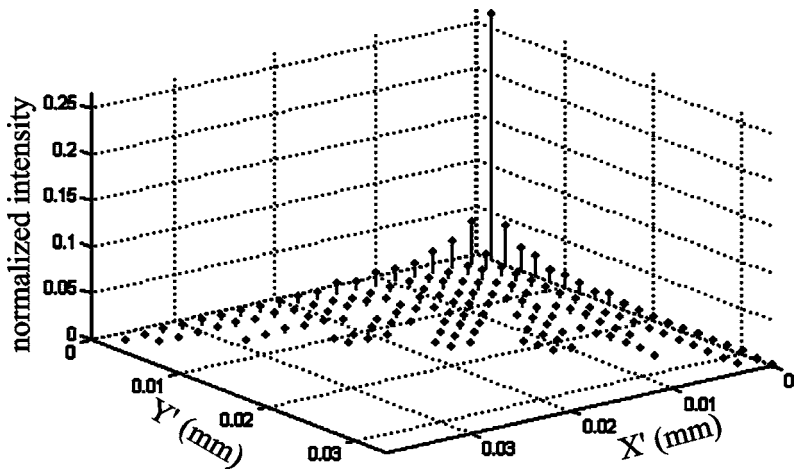

Fig. 13 PSF of the (0, 0) field of view.

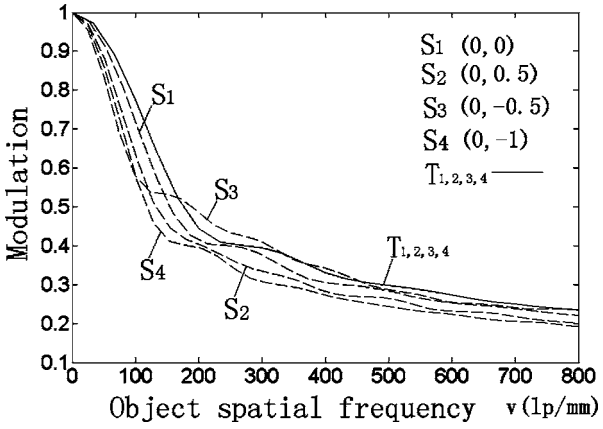

Fig. 15 The MTF curves with different fields along the *Y* axis.

resents the power density along the X' (or Y') coordinate. Figure 13 shows the PSF in the field of view at (0, 0).

Since this system is off axis and severely asymmetric, MTF curves of different field of view in the *X* and *Y* directions are very different. In Fig. 14 and Fig. 15, *T* represents the MTF in the tangential direction, and *S* represents that in the sagittal direction. From Fig. 14 and Fig. 15 we can see that the imaging quality within the $(0.5,-1.0)$ field of view is satisfactory, and a resolution of 5 μm can be obtained in object space.

5 Conclusions

From the preceding analysis we conclude that an optimized KBA x-ray microscope is off axis and severely asymmetrical, with insufficient parameters for correcting all aberrations. Although astigmatism is eliminated, with increasing field of view field obliquity becomes more and more severe and spherical aberration and coma persist. As a result, its effective field is restricted. The estimated resolution for the KBA optics discussed is $\approx$5 μm within a ±1-mm field of view.

Acknowledgments

The authors would like to thank Prof. Zhongli Liu, Prof. Zhijian Zheng, and Dr. Yongkun Ding of the National Key Laboratory of Laser Fusion for their support and assistance.

References

1. J. Hu, *Introduction to Optical Engineering*, pp. 158–164, 800–811, Dalian Univ. of Technology Press, Dalian, China (2002).
2. A. H. Compton, *Philos. Mag.* **45**, 1121–1131 (1923).
3. P. Kirkpatrick and A. B. Baez, "Formation of optical images by x-rays," *J. Opt. Soc. Am.* **38**, 766–774 (1948).
4. W. H. Wolter, "Spiegelsysteme streifenden Einfalls als abbildende Optiken für Röhtgenstrahlen," *Ann. Phys.* **10**, 94–114 (1952).
5. R. Sauneuf, J.-M. Dalmasso, T. Jalinaud, and J. P. LeBreton, "Large-field high-resolution x-ray microscope for studying laser plasmas," *Rev. Sci. Instrum.* **68**(9), 3412–3420 (1995).
6. F. Bridou, R. Mercier, A. Raynal, J. Y. Clotaire, C. Colas, P. Fournet, M. Idir, G. Soullié, C. Remond, and P. Troussel, "Large field double Kirkpatrick–Baez microscope with nonperiodic multilayer for laser plasma imaging," *Rev. Sci. Instrum.* **73**(11), 3789–3795 (2002).
7. J. Hu and L. Song, "Roughness effects on the reflectance in the design of a soft x-ray multilayer mirror," *Opt. Precision Eng.* **12**(4), 380–385 (2004).
8. T. Kingetsu and M. Yamamoto, "Growth of short-period epitaxial superlattices for x-ray multilayer mirrors," *Surf. Sci. Rep.* **45**(3), 79–116 (2002).
9. P. Xiang and C. Jin, "Measurement of residual stress in molybdenum/silicon multilayer coatings" (in Chinese), *Opt. Precision Eng.* **11**(1), 62–67 (2003).
10. C. Wang, "Effect of film thickness errors on performance of soft x-ray multilayer" (in Chinese), *Opt. Precision Eng.* **11**(2), 136–138 (2003).
11. J. Hu, L. Zhao, and X. Li, "Design and analysis of x-ray microscope of four mirrors working at grazing incidence" (in Chinese), *J. Optoelectron., Laser* **16**(5), 534–537 (2005).
12. W. J. Smith, *Modern Optical Engineering*, pp. 360–380, McGraw-Hill, New York (2000).

Jiasheng Hu received his MS degree in applied optics in 1966 from Changchun Institute of Optics and Fine Mechanics, Academia Sinica, and became a professor in 1988. He was a visiting scholar and a visiting professor at the University of California, Santa Barbara, from 1980 to 1982 and in 1993, and he is currently a professor at the Dalian University of Technology. Hu has received various awards from the administration of China and the Academia Sinica, including the first prize for research and design of an optical processor for synthetic aperture radar and two second prizes for a laser scanning microscope and a multispectral imaging microscope. He was also named an Excellent Scientist in 1992 and 1997. Hu's main interests are novel imaging techniques, image processing, pattern recognition, and optical system design, and he has published more than 100 papers in these areas. He is a member of SPIE.

Lingling Zhao is a PhD student in the School of Electronic and Information Engineering, Dalian University of Technology. She got her BS and MS degrees from Henan University of Science and Technology. Now she is majoring in signal and information processing.

Xiang Li received his BSc degree in physics from Dalian University of Technology, China, in 2002. He is currently a MS student in the Department of Physics, Dalian University of Technology, China. His research work focuses on x-ray microscopes working at grazing incidence.